Global source apportionment of aerosols into major emission regions and sectors over 1850–2017

Yang Yang[1*], Shaoxuan Mou[1], Hailong Wang[2], Pinya Wang[1], Baojie Li[1], Hong Liao[1]

[1]Joint International Research Laboratory of Climate and Environment Change (ILCEC), Jiangsu Key Laboratory of Atmospheric Environment Monitoring and Pollution Control, Jiangsu Collaborative Innovation Center of Atmospheric Environment and Equipment Technology, School of Environmental Science and Engineering, Nanjing University of Information Science and Technology, Nanjing, Jiangsu, China

[2]Atmospheric, Climate, and Earth Sciences Division, Pacific Northwest National Laboratory, Richland, Washington, USA

*Correspondence to yang.yang@nuist.edu.cn

Abstract

Anthropogenic emissions of aerosols and precursor gases have been changing significantly in the past few decades across the world. In this study, an explicit aerosol source tagging system (EAST) is merged into the Energy Exascale Earth System Model version 1 (E3SMv1) to quantify the variations in anthropogenic aerosol concentrations, source contributions, and their subsequent radiative impact in four major emission regions on the globe during 1850–1980, 1980–2010 and 2010–2017. In North America and Europe, changes in anthropogenic $PM_{2.5}$ were mainly caused by changes in emissions from local energy and industrial sectors. The local industrial sector caused the most increase in $PM_{2.5}$ in East Asia during1980–2010 and decrease during 2010–2017. In South Asia, the increase in energy-related emissions dominated the rise of $PM_{2.5}$ levels during 1980–2017. During 1850–1980, the increases in emissions from North America contributed to the increase in European $PM_{2.5}$ burden by 1.7 mg m^{-2} and the sources from the Europe were also responsible for the $PM_{2.5}$ burden increase in East Asia and South Asia by about 1.0 mg m^{-2}. During 1980–2010, East Asia contributed to an increase of 0.4–0.6 mg m^{-2} in $PM_{2.5}$ burden in North America and Europe, while South Asian contributed about 0.3 mg m^{-2}. During 2010–2017, the contributions from East Asia to the $PM_{2.5}$ burdens in the North America, Europe and South Asia declined by 0.3–0.6 mg m^{-2} due to Clean Air actions in China, while the contributions from South Asia still increased due to the continuous increase in emissions in South Asia. The historical changes in aerosols had an impact on effective radiative forcing through aerosol-radiation interactions (ERF_{ari}). During 1980–2010, a decline in North American aerosols resulted in a positive ERF_{ari} change (warming effect) in Europe and a decline of aerosols in Europe caused a warming effect in

44   Russia and northern China. The changes in ERF_{ari} from the increase and decrease of aerosols

45   in China during 1980–2010 and 2010–2017, respectively, are comparable in magnitude. The

46   continuous aerosol increases in South Asia from 1980 to 2017 resulted in negative ERF_{ari}

47   (cooling) changes in South Asia, Southeast Asia, and southern China.

1. Introduction

Atmospheric aerosols, also known as particulate matter (PM), have significant influences on air quality and human health (Anenberg et al., 2010; Finlayson-Pitts and Pitts, 1997; Li et al., 2017; Pöschl, 2005). Aerosols also affect the energy budget of the earth system by scattering and/or absorbing solar radiation, thus directly affecting the climate (Gao et al., 2022; Yang et al., 2020a, 2023; Wang et al., 2023). Meanwhile, they may act as cloud condensation nuclei and/or ice nuclei, changing cloud characteristics and atmospheric water cycle, which indirectly affect the climate (Liao et al., 2015; Lohmann and Feichter, 2005; Rosenfeld et al., 2008; Yang et al., 2022a). Due to the absorption of solar radiation, aerosol-induced heating can strengthen temperature inversion and increase the atmospheric stability, which inhibits the vertical mixing and transport of aerosols and leads to a further increase in near-surface aerosol concentrations (Chen et al., 2021; Lou et al., 2019). Therefore, knowing the sources of aerosols and their variations have become a vital direction in the field of environmental and atmospheric sciences.

Human activities have a great influence on global aerosol distributions and compositions. For example, many countries have taken various air quality control measures at different stages of their economic development, causing distinct historical temporal changes of aerosol emissions across the world. Since the start of industrialization, anthropogenic emissions of aerosols and precursor gases have substantially increased, which significantly affected the atmospheric environment and the Earth's energy balance (Carslaw et al., 2013). European and North American countries became major contributors of pollutant emissions. Since the 1980s, coal emissions have declined steadily in Europe and North America owing to the legislation

70   and effective environmental policies to reduce local anthropogenic emissions of aerosol and

71   precursor gases (Smith et al., 2011). In contrast to North America and Europe, the coal

72   consumption in China and India has experienced a substantial increase and anthropogenic

73   emissions from these regions continued to rise (Hoesly et al., 2018; Lim et al., 2020). Zheng et

74   al. (2018) also reported that due to active clean air policies and the emission control of power

75   plants and industry, anthropogenic emissions of $PM_{2.5}$ (particulate matter less than 2.5 μm in

76   diameter) from China have significantly decreased by 33% during 2013–2017. However,

77   countries in South Asia still rely on coal and petroleum and thus aerosol emissions from South

78   Asia have kept increasing in recent years (Li et al., 2017).

79   Regional aerosol pollution can be induced by both local emissions and long-range

80   transport of pollutants across regions, countries or even continents, which impose a far-

81   reaching impact on air quality and human health (Akimoto, 2003; Anenberg et al., 2014; Jaffe

82   et al., 1999; Lin et al., 2014; Liu et al., 2009; Zhang et al., 2017). Studies reported that the air

83   quality in Europe is largely impacted by the long-range aerosol transport from North America

84   (Stohl and Trickl, 1999; Yang et al., 2018a, 2020b). Asian anthropogenic emissions in spring

85   also have a significant effect on the aerosol concentrations in North American (Jaffe et al.,

86   1999). Moreover, studies found that air pollution from Africa and Europe moved eastward and

87   merged with Asian pollution, affecting air quality in western North America (Liu et al., 2005;

88   Chin et al., 2007). Yang et al. (2017) also found that remote sources contributed the most to

89   the regions with low emissions through long-range transport, which further impacted the local

90   climate. Therefore, relying on the domestic emission control alone may be insufficient to

91   prevent air pollution due to the long-distance transport of air pollutants (Liu et al., 2009). A

92   study revealed that approximately 12% of global premature deaths caused by $PM_{2.5}$ were

93   related to non-local air pollutants (Zhang et al., 2017). About 16% of premature deaths in India

94   caused by $PM_{2.5}$ were attributed to aerosol transport from external source regions (David et al.,

95   2019). Within each emission source region, aerosols also come from different emission sectors.

96   Many scientific control measures and policies are implemented based on the source attribution

97   of air pollutants from individual sectors. Hence, it is of great significance to quantify source

98   contributions of long-range transport of aerosols from major emission regions of the world as

99   well as aerosols from major emission sectors.

100   Anthropogenic emissions of aerosols and precursor gases have changed significantly in

101   different source regions over the past century. Few studies focus on the source attributions of

102   aerosols across the globe over such a long period of time. In this study, we focus on the changes

103   in aerosols and emission source region and sector contributions in major source regions (i.e.,

104   North America, Europe, East Asia, South Asia) during the three important periods of emission

105   changes since industrialization (1850–1980, 1980–2010 and 2010–2017)   based on the

106   Energy Exascale Earth System Model version 1 (E3SMv1), equipped with an explicit aerosol

107   source tagging system (E3SMv1-EAST).

108   **2. Methods**

109   **2.1. Model description and experimental design**

110   To study variations in historical anthropogenic aerosols in the major source regions, the

111   E3SMv1 developed by US Department of Energy (DOE) (Golaz et al., 2019) is used in this

112   study. The E3SMv1 model is updated on the basis of Community Atmosphere Model version

113   5 (CAM5) in order to explore several key emerging issues in the field of environment and

114 climate, and is a branch of the widely-used Community Earth System Model (CESM) (Rasch

115 et al., 2019). E3SMv1 consists of atmosphere, land surface, ocean, sea ice, and river model

116 components. It features numerous upgrades to aerosol, turbulence, chemical, and cloud-related

117 processes, offering multiple spatial resolution options. The model can run simulations for

118 decades or more at higher resolution to help understand past, present, and future changes in

119 Earth's behavior, and to explore how the atmosphere interacts with other components of the

120 Earth system. Aerosol microphysics and interactions with stratiform clouds are treated with the

121 four-mode Modal Aerosols Module (MAM4) (Liu et al., 2016), which predicts the mass and

122 number concentrations of sulfate, black carbon (BC), primary organic matter (POM),

123 secondary organic aerosol (SOA), marine organic aerosol, mineral dust and sea salt (Wang et

124 al., 2020). EAMv1 applies the "Morrison and Gettelman version 2" (MG2) two-moment bulk

125 microphysics parameterization for stratiform clouds (Gettelman and Morrison, 2015). It allows

126 aerosol-cloud interactions in all stratiform and shallow convective clouds but neglects in deep

127 convective clouds (Rasch et al., 2019). Liquid cloud drop activation is based on Abdul-Razzak

128 and Ghan (2000) and a classical nucleation theory-based ice nucleation parameterization for

129 the heterogeneous ice formation in mixed-phase clouds follows Y. Wang et al. (2014).

130 Hygroscopicity are specified for soluble aerosols to calculate the particle size based on relative

131 humidity. The aerosols are assumed to mix internally in the same aerosol mode and externally

132 between modes when calculating the aerosol optical properties (Ghan and Zaveri, 2007). The

133 model has been applied to investigate the variations in anthropogenic and natural aerosols

134 related to the air-sea interactions (Yang et al., 2022b; Zeng et al., 2021). Compared to the

135 regional model, the E3SMv1 with an aerosol tagging tool introduced in this study is more

136   suitable for the simulation of transboundary and intercontinental transport of aerosols across

137   the globe. In this study, the model is configured at its standard horizontal spatial resolution of

138   approximately 1° with 72 vertical layers.

139   Global emissions of aerosols and precursor gases used in the simulations are obtained

140   from the CMIP6 (the Coupled Model Intercomparison Project Phase 6) datasets (Hoesly et al.,

141   2018; van Marle et al., 2017). However, the anthropogenic emissions in China are replaced

142   with MEIC (Multi-resolution Emission Inventory for China) inventory, which fully considers

143   the implementation of clean air actions over China since the 2010s (Gao et al., 2022, 2023; Li

144   et al., 2021; Zheng et al., 2018). Following previous studies (Ren et al., 2021; Yang et al.,

145   2018a), the near-surface concentrations of $PM_{2.5}$ here are estimated as the sum of sulfate, BC,

146   POM and SOA concentrations. Effective radiative forcing (ERF) refers to the change of the

147   net radiative flux at the top of the atmosphere (TOA) after the external forcing is applied. In

148   this study, ERF due to aerosol-radiation interactions (ERF_{ari}) for the individual tagged source

149   regions is derived as the difference in TOA net radiative fluxes from a pair of diagnostic

150   radiation calculations with and without the particular tagged aerosols from the source regions

151   for the all-sky condition following Ghan (2013).

152   This study focuses on the variations in source region and sector contributions in four major

153   emission regions of the world (North America, Europe, East Asia and South Asia) during the

154   three key historical periods of emission changes (1850–1980, 1980–2010 and 2010–2017).

155   Four simulations with monthly anthropogenic emissions of aerosols and precursors fixed at the

156   1850, 1980, 2010 and 2017 levels, respectively, are conducted. All simulations are performed

157   for one year following 6-month model spin-up. Greenhouse gas concentrations, solar insolation,

158 sea surface temperature and sea ice extent are prescribed at the 2000 levels. The meteorological

159 fields including 3-dimentional temperature, specific humidity, and winds are nudged toward

160 the MERRA-2 (Modern-Era Retrospective Analysis for Research and Applications, version 2)

161 reanalysis (Gelaro et al., 2017) in year 2017 at a 6-hourly relaxation timescale.

162 **2.2. Explicit aerosol source tagging system**

163   Source apportionment aims to quantify the contributions to aerosols from specific sources.

164 To examine the source-receptor relationships of aerosols, we implemented the Explicit Aerosol

165 Source Tagging (EAST) in E3SMv1, which play a critical role in attributing aerosol

166 concentrations to their respective emission sources. The EAST follows the BC source-tagging

167 technique introduced in H. Wang et al. (2014), sulfate source-tagging method used in Yang et

168 al. (2017) and other carbonaceous aerosol-tagging applied in Yang et al. (2018a), which was

169 previously implemented in the Community Atmosphere Model version 5 (CAM5-EAST). This

170 tagging system is different from the traditional emission sensitivity method that zero out or

171 perturb emissions from a given source region or sector in sensitivity simulations along with a

172 baseline simulation, which has to assume a linear response to emission perturbation and

173 requires many additional simulations for estimating the contributions from multiple sources

174 (Wang et al., 2014). EAST independently considers all aerosol physical, chemical, and

175 dynamical processes for each tagged sources through introducing additional aerosol-related

176 variables within one simulation and it does not rely on a linear response to emission

177 perturbations. These capabilities make it physically more accurate and time saving than the

178 sensitivity experiments. This tagging method has previously been adopted in regional models

179 and has now implemented in the global E3SMv1 model to better understand the

180 intercontinental transport from sources outside the regional domain.

181 In this study, totally 18 tags are set for each anthropogenic species of aerosols and

182 precursors. Each of the 4 major source regions, including North America (NAM), Europe

183 (EUR), East Asia (EAS) and South Asia (SAS), has 4 tags for the energy transformation and

184 extraction (ENE), industrial combustion and processes (IND), residential, commercial and

185 other (RCO) and the rest of anthropogenic emission sectors (RST). One tag is assigned to the

186 anthropogenic emissions from rest of the world (ROW) and the last tag is allocated for all the

187 natural/biogenic sources including open biomass burning, volcanic emissions and oceanic

188 emissions.

189 **2.3. Model evaluation**

190 In order to evaluate the performance of E3SMv1 in reproducing the aerosol concentrations,

191 Fig. 2 compares the simulated near-surface $PM_{2.5}$ concentrations with the observations from

192 the Interagency Monitoring of Protected Visual Environments (IMPROVE) over the U.S., the

193 European Monitoring and Evaluation Programme (EMEP) over Europe, the U.S. embassies

194 and consulates in India and the China National Environmental Monitoring Center (CNEMC)

195 over China in year 2017. The model successfully reproduces the spatial distribution of $PM_{2.5}$

196 concentrations, with relatively high concentrations in eastern China, India and low

197 concentrations in the U.S. and Europe. The spatial correlation coefficient (R) between the

198 E3SMv1 simulated $PM_{2.5}$ concentrations and observations is +0.80. The model well reproduces

199 the $PM_{2.5}$ concentrations in the U.S. with the normalized mean biases (NMB) of -11%.

200 However, it largely underestimates the $PM_{2.5}$ concentrations in China and Europe, which has

201   also been revealed in several studies (e.g., Gao et al., 2018; Gao et al., 2023; Navinya et al.,

202   2020; Zeng et al., 2021). This discrepancy is partly because E3SMv1 only considers limited

203   aerosol species (BC, POM, SOA and sulfate) without including nitrate and ammonium aerosols

204   in the aerosol module. On the other hand, the overestimated wet scavenging at the mid- and

205   high latitudes and underestimated gas-to-particle conversion can also lead to the low bias (Zeng

206   et al., 2021). The evaluation in 2010 also shows similar high correlation and biases (Fig. S3).

207   In order to evaluate the model performance in reproducing the historical changes in

208   aerosol concentrations during the important periods of emission changes, the variations in near-

209   surface $PM_{2.5}$ concentrations are compared with observations (Fig. S4) and MERRA-2

210   reanalysis (Fig. S5). The model well reproduces the decreases in $PM_{2.5}$ concentrations in the

211   eastern U.S. and Europe and the increases in East Asia and South Asia during 1980–2010, with

212   the spatial R of 0.78 between model results and MERRA-2 data. The model also well simulates

213   the aerosol decline in North America, Europe, and East Asia and a continuous increase in South

214   Asia during 2010–2017, with the R of 0.81 between model results and observational data.

215   However, the model simulation does capture the increases in $PM_{2.5}$ in southwestern Canada

216   and eastern Russia. It is because the wildfire emissions were kept unchanged during the

217   simulation, while wildfires occurred more frequently in these regions during the analyzed time

218   period (Jolly et al., 2015; Goss et al., 2020), leading to the increases in $PM_{2.5}$ in observations.

219   **3. Results**

220   **3.1. Historical changes in aerosols over major source regions**

221   Figure 3 shows the variations in anthropogenic emissions of sulfur dioxide (SO_2) during

222   the three key periods of historical emission changes from the tagged source regions. Since

223   industrialization, anthropogenic SO_2 emissions had rising trends during 1850–1980, especially

224   in Europe and North America. Due to the implementation of clean air actions in western

225   countries, SO_2 emissions in North America and Europe declined considerably during 1980–

226   2010, while the emissions in East Asia and South Asia continued to increase. After 2010, China

227   issued several clean air policies, which led to significant decreases in anthropogenic SO_2

228   emissions in East Asia, while the SO_2 emissions in South Asia kept increasing during 2010–

229   2017. The changes in anthropogenic BC and organic carbon (OC) emissions are similar to those

230   of SO_2 (shown in Figure S1 and S2).

231   The changes in near-surface mass concentrations (Fig. 4) and column burdens (Fig. 5) of

232   anthropogenic $PM_{2.5}$ contributed by the tagged source regions during the focused three

233   historical time periods follow the corresponding changes in anthropogenic emissions. Column

234   burden refers to the concentration of aerosols contained in the air column above a unit area

235   with a top at 60 km, which can better reflect the aerosol transport within the air column and is

236   more related to the aerosol radiative effect. The near-surface concentration of aerosols

237   represents the concentration of aerosols in the air near the surface (from ~~1000~~ the surface to

238   997 hPa for model layer), which is more related to air quality and human health. Local

239   anthropogenic emission changes drove the $PM_{2.5}$ to reach its peak in 1980 in North America

240   and Europe and then to decrease. The maximum $PM_{2.5}$ appeared in 2010 in East Asia and the

241   anthropogenic $PM_{2.5}$ level continued growing in South Asia during 1850–2017, consistent with

242   previous studies (Dey et al.,2020; Guttikunda et al., 2022; Singh et al.,2023).

243   To explore which aerosol species contributed the most to the changes in $PM_{2.5}$ during the

244   focused three historical time periods, Figs. 6 and 7 illustrate the relative contributions of

245 individual aerosols to the simulated changes in near-surface $PM_{2.5}$ mass concentrations and

246 column burdens, respectively, in four major emission regions. In general, the historical changes

247 in anthropogenic $PM_{2.5}$ were primarily driven by the changes in sulfate. In North America, the

248 contribution of sulfate to near-surface $PM_{2.5}$ concentration (column burden) rose from 7%

249 (11%) in 1850 to 67% (81%) in 1980, then dropped to 52% (67%) in 2017. In Europe, sulfate

250 contribution changed from 24% (34%) in 1850 to 71% (85%) in 1980, then decreased to 50%

251 (68%) in 2017. In East Asia, sulfate contribution changes from 2% (6%) in 1850 to 51% (71%)

252 in 1980, then decreased to 33% (56%) in 2017. It is interesting that the $PM_{2.5}$ levels in East

253 Asia increased during 1980–2010, but the sulfate contribution decreased in this time period. It

254 is because the carbonaceous aerosols increased remarkably, which reduced the fractional

255 contribution of sulfate. The sulfate contribution to $PM_{2.5}$ concentration (column burden)

256 increased throughout the period of 1850–2017, from 2% (5%) to 42% (62%) in South Asia.

257 Note that the carbonaceous aerosols, especially POM, dominated the $PM_{2.5}$ in all four targeted

258 regions in 1850, resulting from the high heating demand from the residential sector.

259 **3.2 Changes in contributions from major source regions and sectors**

260 Figure 8 shows the relative contributions from local and remote anthropogenic sources to

261 the near-surface concentrations and column burdens of $PM_{2.5}$ in the four targeted regions in

262 2010. Local sources dominated the near-surface anthropogenic $PM_{2.5}$ concentrations over the

263 high emission regions including eastern China, eastern U.S. and Indo-Gangetic Plain, with

264 local contributions being higher than 90%. In the regions with low emissions, such as the

265 Tibetan Plateau, the anthropogenic $PM_{2.5}$ concentrations were largely contributed by the long-

266 range transport of aerosols. The spatial distributions of burden contribution are similar to those

267   of corresponding contribution near the surface, but the long-range transport contributed more

268   to the column burden than to the near-surface contribution due to the more efficient pollutant

269   transport in the free troposphere than within the boundary layer. The long-range transport

270   contributes 30%–35% of $PM_{2.5}$ burden in East Asia and South Asia and 50–55% in North

271   America and Europe, much higher than the 10%–25% for the near-surface concentrations over

272   the four targeted regions.

273   Since both local and remote emissions can contribute to the anthropogenic $PM_{2.5}$, it is

274   valuable to know the historical changes in these contributions, especially by the local sources

275   from individual emission sectors and by remote sources from major emission regions. Figure

276   9 illustrates changes in the local source contributions from major emission sectors to the near-

277   surface concentrations and column burdens of $PM_{2.5}$ during 1850–2017. In North America and

278   Europe, the historical changes in anthropogenic $PM_{2.5}$ were largely induced by changes in

279   emissions from the local energy (ENE) sector, followed by the industry (IND) sector, which

280   increased before 1980 and decreased afterward. In East Asia, ENE, IND and residential (RCO)

281   sector emissions all had significant contributions to the increases in $PM_{2.5}$ concentration and

282   burden from1850 to1980. Then the contribution from local IND sector showed the largest

283   increases from 1980 to 2010 and decreases from 2010 to 2017. In South Asia, the

284   anthropogenic $PM_{2.5}$ increases from 1850 to 1980 were mainly attributed to the RCO emission

285   increases. After that, increases in ENE emissions dominated the rising $PM_{2.5}$ levels in South

286   Asia during 1980–2017.

287   Figure 10 presents changes in remote emission contributions from the tagged source

288   regions to the column burdens of $PM_{2.5}$ during 1850–2017. The contributions from long-range

transport to the near-surface concentrations and their historical variations over the four major emissions regions are relatively small, which were also reported in previous studies (e.g., Yang et al., 2018b) and are not discussed here. During 1850–1980, the long-range transport contributions to the $PM_{2.5}$ burdens show increases and the contributions from ROW increased the most among the tagged source regions over all four targeted receptor regions. Note that aerosol emissions from North America contributed to the increase in European $PM_{2.5}$ burden by 1.7 mg m^{-2} and sources from Europe were also responsible for the $PM_{2.5}$ burden increase by 1.0 mg m^{-2} in East Asia and 1.1 mg m^{-2} in South Asia. During 1980–2010, the long-range transport from North America and Europe decreased, but that from East Asia and South Asia increased. East Asia contributed 0.4–0.6 mg m^{-2} to the $PM_{2.5}$ burden increases in North America, while Europe and South Asia contributed about 0.3 mg m^{-2}. In East Asia, 1.6 mg m^{-2} of the $PM_{2.5}$ burden increase was attributed to South Asian sources and 0.8 mg m^{-2} of the $PM_{2.5}$ burden increase in South Asia during this time period was due to increases in East Asian emissions. From 2010 to 2017, owing to the clean air actions in China, contributions from East Asia to the $PM_{2.5}$ burdens in the other three targeted regions decreased by 0.3–0.6 mg m^{-2}. However, due to the continuous increases in South Asian emissions, South Asia still contributed to the $PM_{2.5}$ burden increase in East Asia by 0.4 mg m^{-2} during this short time period.

3.3 Changes in effective radiative forcing due to aerosol-radiation interactions

The variation in aerosols can have a significant impact on ERF through aerosol-radiation and aerosol-cloud interactions. Figure 11 shows changes in ERF due to aerosol-radiation interactions (ERF_{ari}) at the top of the atmosphere (TOA) that can be attributed to changes in

311   anthropogenic emissions from the tagged regions in the three key periods during 1850–2017.

312   Due to the increases in aerosols from 1850 to 1980, a large negative ERF_{ari} was located over

313   the major source regions and their downwind areas, with maximum ERF_{ari} changes being larger

314   than 2 W m^{-2} over eastern U.S., Europe and eastern China. In 2010, there were positive ERF_{ari}

315   changes (warming effect) by a maximum of 2 W m^{-2} in North America and Europe compared

316   to 1980, which were due to the decreases in anthropogenic aerosols in these two regions. The

317   positive ERF_{ari} changes due to the decrease in North American aerosols extended across the

318   North Atlantic and caused an increase in incoming radiation by up to 0.5 W m^{-2} in Europe.

319   Similarly, the decrease in aerosols from Europe also led to a positive ERF_{ari} change by up to

320   0.5 W m^{-2} in the downwind regions including Russia and northern China during 1980–2010.

321   This is also revealed by previous studies that aerosol reduction has caused fast warming in

322   downwind regions (Urdiales-Flores et al., 2023). Increases in aerosols in China during 1980–

323   2010 and decreases during 2010–2017 produced negative (cooling) and positive (warming)

324   changes in ERF_{ari}, respectively, over eastern China and North Pacific, which largely

325   contradicted each other. The continuously growing aerosols in South Asia induced negative

326   ERF_{ari} changes (cooling) in South Asia, Southeast Asia and southern China during both 1980–

327   2010 and 2010–2017. Note that in this study we only quantify the ERF_{ari} for the major emission

328   regions based on the source tagging technique. The quantification of ERF due to aerosol-cloud

329   interactions (ERF_{aci}) requires additional simulations, which could be further examined in future

330   studies.

331   **4. Conclusions and Discussions**

332   Since the start of industrialization, aerosols have changed significantly in different regions

333   of the world driven by global economic development and air pollution control measures. It is

334   of great significance to quantify the contributions of aerosols from major emission source

335   regions and sectors during the key periods of substantial emission changes. In this study, the

336   Explicit Aerosol Source Tagging (EAST) technique is implemented in E3SMv1 to quantify the

337   variations in the concentrations, source contributions, and the subsequent effective radiative

338   forcing of anthropogenic aerosols in four major source regions (NAM, EUR, EAS and SAS)

339   during three key historical periods of emission changes (1850–1980, 1980–2010 and 2010–

340   2017).

341   Following the corresponding anthropogenic emission changes, $PM_{2.5}$ concentrations

342   reached its peak in 1980 in North America and Europe, while the peak of $PM_{2.5}$ in East Asia

343   occurred in 2010. The $PM_{2.5}$ from anthropogenic sources in South Asia continued growing

344   during 1850–2017. These changes in anthropogenic $PM_{2.5}$ were primarily dominated by

345   changes in sulfate aerosol. In North America and Europe, historical changes in anthropogenic

346      $PM_{2.5}$ were mainly caused by changes in emissions from local energy sector, followed by the

347   industrial sector, which increased from 1850 to 1980 and decreased afterward. In East Asia,

348   energy, industrial, and residential emissions contributed significantly to the increase in $PM_{2.5}$

349   from 1850 to 1980, then the local industrial sector caused the most increase from 1980 to 2010,

350   and declined from 2010 to 2017. For South Asia, the increase in $PM_{2.5}$ was mainly due to

351   emission changes in the residential sector from 1850 to 1980, then the increase in energy-

352   related emissions became dominant to the rise of $PM_{2.5}$ levels during 1980–2017.

353   Regional aerosol pollution comes from both local emissions and long-range transport of

354   remote emissions. Local emissions contribute the most in regions with high emissions, while

355   in regions with low emissions the long-distance transport plays an important role. Due to the

356   more efficient transport of air pollutants in the free troposphere, contributions of long-range

357   transport to column burden are greater than to the near-surface concentration over all four

358   targeted receptor regions. From 1850 to 1980, increases in emissions from North America

359   contributed to the increase in European $PM_{2.5}$ burden by 1.7 mg m^{-2} and emissions from Europe

360   were also responsible for the $PM_{2.5}$ burden increase by 1.0 mg m^{-2} in East Asia and 1.1 mg m^{-}

361   ^{2} in South Asia. From 1980 to 2010, the long-range transport from North America and Europe

362   decreased, while those from East Asia and South Asia increased. East Asia contributed 0.4–

363   0.6 mg m^{-2} to the $PM_{2.5}$ burden increases in North America, while Europe and South Asia

364   contributed about 0.3 mg m^{-2}. In East Asia, 1.6 mg m^{-2} of the $PM_{2.5}$ burden increase was

365   attributed to South Asian sources and 0.8 mg m^{-2} of the $PM_{2.5}$ burden increase in South Asia

366   during this time period was due to the increases in East Asian emissions. From 2010 to 2017,

367   the contributions from East Asia to the $PM_{2.5}$ burdens in the other three targeted regions

368   declined by 0.3–0.6 mg m^{-2} due to Clean Air actions in China. However, due to the continuous

369   increase of emissions in South Asia, the $PM_{2.5}$ burden in East Asia still increased by 0.4 mg m^{-}

370   ^{2}.

371   Changes in aerosols can have a significant impact on ERF, which further imposes an

372   impact on climate. Large negative ERF_{ari} appeared over the major source regions and their

373   downwind areas during 1850–1980 due to the increases in aerosol emissions, with maximum

374   ERF_{ari} changes being larger than 2 W m^{-2} over eastern North America, Europe and eastern

375   China. From 1980 to 2010, a positive ERF_{ari} change caused by a decline in North American

376   aerosols extended over the North Atlantic, resulting in a warming of up to 0.5 W m^{-2} in Europe.

377   Meanwhile, a decline of aerosols in Europe also caused a warming of up to 0.5 W m^{-2} in Russia

378   and northern China. The changes in ERF_{ari} from the increase (from 1980 to 2010) and decrease

379   (from 2010 to 2017) of aerosols in China had an opposite sign. The continuous aerosol

380   increases in South Asia from 1980 to 2017 resulted in negative ERF_{ari} changes in South Asia,

381   Southeast Asia, and southern China.

382   This study provides an in-depth analysis of historical changes in anthropogenic aerosol

383   concentrations, compositions, source contributions and radiative impacts in the four major

384   emission source regions of the globe, which has important implications for the pollution

385   prevention/control measures and decision making for global collaboration. The spatial

386   distribution and changes in anthropogenic aerosols are similar to those reported in previous

387   studies (Hoesly, et al., 2018; Lim, et al., 2020). However, we also note that the E3SMv1 model

388   underestimates the near-surface $PM_{2.5}$ concentrations in Europe and East Asia, which could

389   lead to an underestimate of the corresponding radiative and climate impact. Our analysis

390   focuses on aerosols from anthropogenic emissions; however, with the increasing attention to

391   air quality in many countries around the world, anthropogenic aerosol concentrations are

392   declining and contributions from biomass burning aerosols are becoming more and more

393   important. The source contributions and impacts of biomass burning aerosols will be

394   investigated in our future work. Also, this study only quantifies the ERF_{ari} for individual major

395   emission regions based on the source tagging technique and radiation diagnostic calculations.

396   The quantification of ERF_{aci} requires additional simulations, which could be further examined

397   in future studies.

398 ***Author contributions.*** YY designed the research, added the tagging code and performed

399 simulations; SM analyzed the data. All authors including HW, PW, and HL discussed the

400 results and wrote the paper.

401

402 ***Code and data availability.*** The E3SMv1 model is available at https://github.com/E3SM-

403 Project/E3SM(last access:1 October 2022) (https://doi.org/10.11578/E3SM/dc.20180418.36;

404 E3SM Project, 2018). Our results can be made available upon request.

405

406 ***Acknowledgments.*** HW acknowledges the support by the U.S. Department of Energy (DOE),

407 Office of Science, Office of Biological and Environmental Research (BER), as part of the

408 Earth and Environmental System Modeling program. The Pacific Northwest National

409 Laboratory (PNNL) is operated for DOE by the Battelle Memorial Institute under contract

410 DE-AC05-76RLO1830.

411

412 ***Financial support.*** This study was supported by the National Key Research and

413 Development Program of China (grant 2020YFA0607803 ~~and 2019YFA0606800~~), ~~the~~

414 ~~National Natural Science Foundation of China (grant 41975159),~~ Jiangsu Science Fund for

415 Distinguished Young Scholars (grant BK20211541), and the Jiangsu Science Fund for

416 Carbon Neutrality (grant ~~no.~~ BK20220031).

417

418 ***Conflict of interest.***

419 At least one of the (co-)authors is a member of the editorial board of ACP.

420 **References**
421
422 Abdul-Razzak, H. and Ghan, S. J.: A parameterization of aerosol activation, 2. Multiple
423   aerosol types, J. Geophys. Res., 105, 6837– 6844,
424   https://doi.org/10.1029/1999JD901161, 2000.
425
426 Akimoto, H.: Global Air Quality and Pollution, Science, 302, 1716–1719,
427   https://doi.org/10.1126/science.1092666, 2003.
428
429 Anenberg, S. C., Horowitz, L. W., Tong, D. Q., and West, J. J.: An Estimate of the Global
430   Burden of Anthropogenic Ozone and Fine Particulate Matter on Premature Human
431   Mortality Using Atmospheric Modeling, Environ. Health Perspect., 118, 1189–1195,
432   https://doi.org/10.1289/ehp.0901220, 2010.
433
434 Anenberg, S. C., West, J. J., Yu, H., Chin, M., Schulz, M., Bergmann, D., Bey, I., Bian, H.,
435   Diehl, T., Fiore, A., Hess, P., Marmer, E., Montanaro, V., Park, R., Shindell, D.,
436   Takemura, T., and Dentener, F.: Impacts of intercontinental transport of anthropogenic
437   fine particulate matter on human mortality, Air. Qual. Atmos. Health., 7, 369–379,
438   https://doi.org/10.1007/s11869-014-0248-9, 2014.
439
440 Carslaw, K. S., Gordon, H., Hamilton, D. S., Johnson, J. S., Regayre, L. A., Yoshioka, M.,
441   and Pringle, K. J.: Aerosols in the Pre-industrial Atmosphere, Curr. Clim. Change Rep.,
442   3, 1–15, https://doi.org/10.1007/s40641-017-0061-2, 2017.
443
444 Chen, D., Liao, H., Yang, Y., Chen, L., and Wang, H.: Simulated aging processes of black
445   carbon and its impact during a severe winter haze event in the Beijing-Tianjin-Hebei
446   region, Sci. Total Environ., 755, 142712,
447   https://doi.org/10.1016/j.scitotenv.2020.142712, 2021.
448
449 Chin, M., Diehl, T., Ginoux, P., and Malm, W.: Intercontinental transport of pollution and
450   dust aerosols: implications for regional air quality, Atmos. Chem. Phys., 7, 5501–5517,
451   https://doi.org/10.5194/acp-7-5501-2007, 2007.
452
453 David, L. M., Ravishankara, A. R., Kodros, J. K., Pierce, J. R., Venkataraman, C., and
454   Sadavarte, P.: Premature mortality due to $PM_{2.5}$ over India: Effect of atmospheric
455   transport and anthropogenic emissions, Geohealth, 3, 2–10,
456   https://doi.org/10.1029/2018GH000169, 2019.
457
458 Dey, S., Purohit, B., Balyan, P., Dixit, K., Bali, K., Kumar, A., Imam, F., Chowdhury, S.,
459   Ganguly, D., Gargava, P., and Shukla, V. K.: A satellite-based high-resolution (1-km)
460   ambient $PM_{2.5}$ database for India over two decades (2000–2019): applications for air
461   quality management, Remote Sens., 12, 3872, https://doi.org/10.3390/rs12233872, 2022.
462

Finlayson-Pitts, B. J., and Pitts, J. N.: Tropospheric Air Pollution: Ozone, Airborne Toxics, Polycyclic Aromatic Hydrocarbons, and Particles, Science, 276, 1045–1051, https://doi.org/10.1126/science.276.5315.1045, 1997.

Gao, M., Beig, G., Song, S., Zhang, H., Hu, J., Ying, Q., Liang, F., Liu, Y., Wang, H., Lu, X., Zhu, T., Carmichael, G. R., Nielsen, C. P., McElroy, M. B.: The impact of power generation emissions on ambient $PM_{2.5}$ pollution and human health in China and India, Environ. Int., 121, 250-259, https://doi.org/10.1016/j.envint.2018.09.015, 2018.

Gao, J., Yang, Y., Wang, H., Wang, P., Li, H., Li, M., Ren, L., Yue, X., and Liao, H.: Fast climate responses to emission reductions in aerosol and ozone precursors in China during 2013–2017, Atmos. Chem. Phys., 22, 7131–7142, https://doi.org/10.5194/acp-22-7131-2022, 2022.

Gao, J., Yang, Y., Wang, H., Wang, P., Li, B., Li, J., Wei, J., Gao, M., and Liao, H.: Climate responses in China to domestic and foreign aerosol changes due to clean air actions during 2013–2019, npj Clim. Atmos. Sci., 6, 160, https://doi.org/10.1038/s41612-023-00488-y, 2023.

Gelaro, R., McCarty, W., Suárez, M. J., Todling, R., Molod, A., Takacs, L., Randles, C. A., Darmenov, A., Bosilovich, M. G., Reichle, R., Wargan, K., Coy, L., Cullather, R., Draper, C., Akella, S., Buchard, V., Conaty, A., da Silva, A. M., Gu, W., Kim, G., Koster, R., Lucchesi, R., Merkova, D., Nielsen, J. E., Partyka, G., Pawson, S., Putman, W., Rienecker, M., Schubert, S. D., Sienkiewicz, M., and Zhao, B.: The Modern-Era Retrospective Analysis for Research and Applications, Version 2 (MERRA-2), J. Climate, 30, 5419–5454, https://doi.org/10.1175/JCLI-D-16-0758.1, 2017.

Ghan, S. J.: Technical Note: Estimating aerosol effects on cloud radiative forcing, Atmos. Chem. Phys., 13, 9971–9974, https://doi.org/10.5194/acp-13-9971-2013, 2013.

Ghan, S. J. and Zaveri, R. A.: Parameterization of optical properties for hydrated internally mixed aerosol, J. Geophys. Res.-Atmos., 112, D10201, https://doi.org/10.1029/2006JD007927, 2007.

Golaz, J. C., Caldwell, P. M., Van Roekel, L. P., Petersen, M. R., Tang, Q., Wolfe, J. D., Abeshu, G., Anantharaj, V., Asay-Davis, X. S., Bader, D. C., Baldwin, S. A., Bisht, G., Bogenschutz, P. A., Branstetter, M., Brunke, M. A., Brus, S. R., Burrows, S. M., Cameron-Smith, P. J., Donahue, A. S., Deakin, M., Easter, R. C., Evans, K. J., Feng, Y., Flanner, M., Foucar, J. G., Fyke, J. G., Griffin, B. M., Hannay, C., Harrop, B. E., Hoffman, M. J., Hunke, E. C., Jacob, R. L., Jacobsen, D. W., Jeffery, N., Jones, P. W., Keen, N. D., Klein, S. A., Larson, V. E., Leung, L. R., Li, H. Y., Lin, W., Lipscomb, W. H., Ma, P., Mahajan, S., Maltrud, M. E., Mametjanov, A., McClean, J. L., McCoy, R. B., Neale, R. B., Price, S. F., Qian, Y., Rasch, P. J., Eyre, J. E. J. R., Riley, W. J., Ringler, T. D., Roberts, A. F., Roesler, E. L., Salinger, A. G., Shaheen, Z., Shi, X.,

Singh, B., Tang, J., Taylor, M. A., Thornton, P. E., Turner, A. K., Veneziani, M., Wan, H., Wang, H., Wang, S., Williams, D. N., Wolfram, P. J., Worley, P. H., Xie, S., Yang Y., Yoon, J., Zelinka, M. D., Zender, C. S., Zeng, X., Zhang, C., Zhang, K., Zhang, Y., Zheng, X., Zhou, T., and Zhu, Q.: The DOE E3SM Coupled Model Version 1: Overview and Evaluation at Standard Resolution, J. Adv. Model. Earth Syst., 11, 2089–2129. https://doi.org/10.1029/2018MS001603, 2019.

Goss, M., Swain, D. L., Abatzoglou, J. T., Sarhadi, A., Kolden, C. A., Williams A. P., and Diffenbaugh, N. S.: Climate change is increasing the likelihood of extreme autumn wildfire conditions across California, Environ. Res. Lett., 15, 094016, https://doi.org/10.1088/1748-9326/ab83a7, 2020.

Guttikunda, S., and Nishadh, K. A.: Evolution of India's $PM_{2.5}$ pollution between 1998 and 2020 using global reanalysis fields coupled with satellite observations and fuel consumption patterns, Environ. Sci. Atmos., 2, 1502-1515, https://doi.org/10.1039/D2EA00027J, 2022.

Hoesly, R. M., Smith, S. J., Feng, L., Klimont, Z., Janssens-Maenhout, G., Pitkanen, T., Seibert, J. J., Vu, L., Andres, R. J., Bolt, R. M., Bond, T. C., Dawidowski, L., Kholod, N., Kurokawa, J., Li, M., Liu, L., Lu, Z., Moura, M. C. P., O'Rourke, P. R., and Zhang, Q.: Historical (1750–2014) anthropogenic emissions of reactive gases and aerosols from the Community Emissions Data System (CEDS), Geosci. Model Dev., 11, 369–408, https://doi.org/10.5194/gmd-11-369-2018, 2018.

Jaffe, D., Anderson, T., Covert, D., Kotchenruther, R., Trost, B., Danielson, J., Simpson, W., Berntsen, T., Karlsdottir, S., Blake, D., Harris, J., Carmichael, G., and Uno, I.: Transport of Asian air pollution to North America, Geophys. Res. Lett., 26, 711–714, https://doi.org/10.1029/1999GL900100, 1999.

Jolly, W. M., Cochrane, M. A., Freeborn, P. H., Holden, Z. A., Brown, T. J., Williamson, G. J., and Bowman, D. M. J. S.: Climate-induced variations in global wildfire danger from 1979 to 2013, Nat. Commun., 6, 7537, https://doi.org/10.1038/ncomms8537, 2015.

Li, C., McLinden, C., Fioletov, V., Krotkov, N., Carn, S., Joiner, J., Streets, D., He, H., Ren, X., Li, Z., and Dickerson, R.: India Is Overtaking China as the World's Largest Emitter of Anthropogenic Sulfur Dioxide, Sci. Rep., 7, 14304, https://doi.org/10.1038/s41598-017-14639-8, 2017.

Li, H., Yang, Y., Wang, H., Li, B., Wang, P., Li, J., and Liao, H.: Constructing a spatiotemporally coherent long-term $PM_{2.5}$ concentration dataset over China using a machine learning approach, Sci. Total Environ., 765, 144263, https://doi.org/10.1016/j.scitotenv.2020.144263, 2021.

550   Liao, H., Chang, W., and Yang, Y.: Climatic effects of air pollutants over China: A review,
551   Adv. Atmos. Sci., 32, 115–139, https://doi.org/10.1007/s00376-014-0013-x, 2015.
552
553   Lim, C.-H., Ryu, J., Choi, Y., Jeon, S. W., and Lee, W.-K.: Understanding global PM2.5
554   concentrations and their drivers in recent decades (1998–2016), Environ. Int., 144,
555   106011, https://doi.org/10.1016/j.envint.2020.106011, 2020.
556
557   Lin, J., Pan, D., Davis, S. J., Zhang, Q., He, K., Wang, C., Streets, D. G., Wuebbles, D. J.,
558   and Guan, D.: China's international trade and air pollution in the United States, Proc.
559   Natl. Acad. Sci., 111, 1736–1741, https://doi.org/10.1073/pnas.1312860111, 2014.
560
561   Liu, J., and Mauzerall, D.: Estimating the average time for inter-continental transport of air
562   pollutants, Geophys. Res. Lett., 32, L11814, https://doi.org/10.1029/2005GL022619,
563   2005.
564
565   Liu, J., Mauzerall, D. L., Horowitz, L. W., Ginoux, P., and Fiore, A. M.: Evaluating inter-
566   continental transport of fine aerosols: (1) Methodology, global aerosol distribution and
567   optical depth, Atmos. Environ., 43, 4327–4338,
568   https://doi.org/10.1016/j.atmosenv.2009.03.054, 2009.
569
570   Lohmann, U., and Feichter, J.: Global indirect aerosol effects: a review, Atmos. Chem. Phys.,
571   5, 715–737, https://doi.org/10.5194/acp-5-715-2005, 2005.
572
573   Lou, S., Yang, Y., Wang, H., Smith, S. J., Qian, Y., and Rasch, P. J.: Black carbon amplifies
574   haze over the North China Plain by weakening the East Asian winter monsoon,
575   Geophys. Res. Lett., 46, 452–460, https://doi.org/10.1029/2018GL080941, 2019.
576
577   Navinya, C. D., Vinoj, V. and Pandey, S. K.: Evaluation of $PM_{2.5}$ Surface Concentrations
578   Simulated by NASA's MERRA Version 2 Aerosol Reanalysis over India and its relation
579   to the Air Quality Index, Aerosol Air Qual. Res., 20, 1329–1339,
580   https://doi.org/10.4209/aaqr.2019.12.0615, 2020.
581
582   Pöschl, U.: Atmospheric Aerosols: Composition, Transformation, Climate and Health
583   Effects, Angew. Chem. Int. Ed., 44, 7520–7540,
584   https://doi.org/10.1002/anie.200501122, 2005.
585
586   Rasch, P. J., Xie, S., Ma, P.-L., Lin, W., Wang, H., Tang, Q., Burrows, S. M., Caldwell, P.,
587   Zhang, K., Easter, R. C., Cameron-Smith, P., Singh, B., Wan, H., Golaz, J.-C., Harrop,
588   B. E., Roesler, E., Bacmeister, J., Larson, V. E., Evans, K. J., Qian, Y., Taylor, M.,
589   Leung, L. R., Zhang, Y., Brent, L., Branstetter, M., Hannay, C., Mahajan, S.,
590   Mametjanov, A., Neale, R., Richter, J. H., Yoon, J.-H., Zender, C. S., Bader, D.,
591   Flanner, M., Foucar, J. G., Jacob, R., Keen, N., Klein, S. A., Liu, X., Salinger, A. G.,
592   Shrivastava, M., and Yang, Y.: An overview of the atmospheric component of the

Energy Exascale Earth System Model, J. Adv. Model. Earth Sy., 11, 2377–2411, https://doi.org/10.1029/2019MS001629, 2019.

Ren, L., Yang, Y., Wang, H., Wang, P., Chen, L., Zhu, J., and Liao, H.: Aerosol transport pathways and source attribution in China during the COVID-19 outbreak, Atmos. Chem. Phys., 21, 15431–15445, https://doi.org/10.5194/acp-21-15431-2021, 2021.

Rosenfeld, D., Lohmann, U., Raga, G. B., Kulmala, M., Fuzzi, S., Reissell, A., and Andreae, M. O.: Flood or Drought: How Do Aerosols Affect Precipitation?, Science, 321, 1309–1313, https://doi.org/10.1126/science.1160606, 2008.

Singh, T., Matsumi, Y., Nakayama, T., Hayashida, S., Patra, P. K., Yasutomi, N., Kajino, M., Yamaji, K., Khatri, P., Takigawa, M., Araki, H., Kurogi, Y., Kuji, M., Muramatsu, K., Imasu, R., Ananda, A., Arbain, A. A., Ravindra, K., Bhardwaj, S., Kumar, S., Mor, S., Dhaka, S. K., Dimri, A. P., Sharma, A., Singh, N., Bhatti, M. S., Yadav, R., Vatta, K., and Mor, S.: Very high particulate pollution over northwest India captured by a high-density in situ sensor network, Sci. Rep., 13, 13201, https://doi.org/10.1038/s41598-023-39471-1, 2023.

Smith, S. J., van Aardenne, J., Klimont, Z., Andres, R. J., Volke, A., and Arias, S. D.: Anthropogenic sulfur dioxide emissions: 1850–2005, Atmos. Chem. Phys., 11, 1101–1116, https://doi.org/10.5194/acp-11-1101-2011, 2011.

Stohl, A., and Trickl, T.: A textbook example of long-range transport: Simultaneous observation of ozone maxima of stratospheric and North American origin in the free troposphere over Europe, J. Geophys. Res., 104, 30445–30462, https://doi.org/10.1029/1999JD900803, 1999.

Urdiales-Flores, D., Zittis, G., Hadjinicolaou, P., Osipov, S., Klingmüller, K., Mihalopoulos, N., Kanakidou, M., Economou, T., and Lelieveld, J.: Drivers of accelerated warming in Mediterranean climate-type regions, npj. Clim. Atmos. Sci., 6, 97, https://doi.org/10.1038/s41612-023-00423-1, 2023.

van Marle, M. J. E., Kloster, S., Magi, B. I., Marlon, J. R., Daniau, A.-L., Field, R. D., Arneth, A., Forrest, M., Hantson, S., Kehrwald, N. M., Knorr, W., Lasslop, G., Li, F., Mangeon, S., Yue, C., Kaiser, J. W., and van der Werf, G. R.: Historic global biomass burning emissions for CMIP6 (BB4CMIP) based on merging satellite observations with proxies and fire models (1750–2015), Geosci. Model Dev., 10, 3329–3357, https://doi.org/10.5194/gmd-10-3329-2017, 2017.

Wang, H., Rasch, P. J., Easter, R. C., Singh, B., Zhang, R., Ma, P.-L., Qian, Y., Ghan, S. J., and Beagley, N.: Using an explicit emission tagging method in global modeling of source-receptor relationships for black carbon in the Arctic: Variations, sources, and

transport pathways, J. Geophys. Res. Atmos., 119, 12888–12909, https://doi.org/10.1002/2014JD022297, 2014.

Wang, H., Easter, R. C., Zhang, R., Ma, P.-L., Singh, B., Zhang, K., Ganguly, D., Rasch, P. J., Burrows, S. M., Ghan, S. J., Lou, S., Qian, Y., Yang, Y., Feng, Y., Flanner, M., Leung, L. R., Liu, X., Shrivastava, M., Sun, J., Tang, Q., Xie, S., and Yoon, J.-H.: Aerosols in the E3SM Version 1: New developments and their impacts on radiative forcing, J. Adv. Model. Earth Syst., 12, e2019MS001851, https://doi.org/10.1029/2019MS001851, 2020.

Wang, P., Yang, Y., Xue, D., Ren, L., Tang, J., Leung, L. R., and Liao, H.: Aerosols overtake greenhouse gases causing a warmer climate and more weather extremes toward carbon neutrality, Nat. Commun., 14, 7257, https://doi.org/10.1038/s41467-023-42891-2, 2023.

Wang, Y., Liu, X., Hoose, C., and Wang, B.: Different contact angle distributions for heterogeneous ice nucleation in the Community Atmospheric Model version 5, Atmos. Chem. Phys., 14, 10411–10430, https://doi.org/10.5194/acp-14-10411-2014, 2014.

Yang, Y., Wang, H., Smith, S. J., Easter, R., Ma, P.-L., Qian, Y., Yu, H., Li, C., and Rasch, P. J.: Global source attribution of sulfate concentration and direct and indirect radiative forcing, Atmos. Chem. Phys., 17, 8903–8922, https://doi.org/10.5194/acp-17-8903-2017, 2017.

Yang, Y., Wang, H., Smith, S. J., Zhang, R., Lou, S., Qian, Y., Ma, P., and Rasch P. J.: Recent intensification of winter haze in China linked to foreign emissions and meteorology, Sci. Rep., 8, 2107, https://doi.org/10.1038/s41598-018-20437-7, 2018a.

Yang, Y., Wang, H., Smith, S. J., Zhang, R., Lou, S., Yu, H., Li, C., and Rasch, P. J.: Source Apportionments of Aerosols and Their Direct Radiative Forcing and Long-Term Trends Over Continental United States, Earth's Future, 6, 793–808, https://doi.org/10.1029/2018EF000859, 2018b.

Yang, Y., Ren, L., Li, H., Wang, H., Wang, P., Chen, L., Yue, X., and Hong, L.: Fast climate responses to aerosol emission reductions during the COVID-19 pandemic, Geophys. Res. Lett., 47, e2020GL089788, https://doi.org/10.1029/2020GL089788, 2020a.

Yang, Y., Lou, S., Wang, H., Wang, P., and Liao, H.: Trends and source apportionment of aerosols in Europe during 1980–2018, Atmos. Chem. Phys., 20, 2579–2590, https://doi.org/10.5194/acp-20-2579-2020, 2020b.

Yang, Y., Ren, L., Wu, M., Wang, H., Song, F., Leung, L. R., Hao, X., Li, J., Chen, L., Li, H., Zeng, L., Zhou, Y., Wang, P., Liao, H., Wang, J., and Zhou, Z.-Q.: Abrupt emissions reductions during COVID-19 contributed to record summer rainfall in China, Nat. Commun., 13, 959, https://doi.org/10.1038/s41467-022-28537-9, 2022a

680

681   Yang, Y., Zeng, L., Wang, H., Wang, P., and Liao, H.: Dust pollution in China affected by
682   different spatial and temporal types of El Niño, Atmos. Chem. Phys., 22, 14489–14502,
683   https://doi.org/10.5194/acp-22-14489-2022, 2022b.
684

685   Yang, Y., Zeng, L., Wang, H., Wang, P., and Liao, H.: Climate effects of future aerosol
686   reductions for achieving carbon neutrality in China, Sci. Bull., 68, 902–905,
687   https://doi.org/10.1016/j.scib.2023.03.048, 2023..
688

689   Zeng, L., Yang, Y., Wang, H., Wang, J., Li, J., Ren, L., Li, H., Zhou, Y., Wang, P., and Liao,
690   H.: Intensified modulation of winter aerosol pollution in China by El Niño with short
691   duration, Atmos. Chem. Phys., 21, 10745–10761, https://doi.org/10.5194/acp-21-10745-
692   2021, 2021.
693

694   Zhang, Q., Jiang, X., Tong, D., Davis, S. J., Zhao, H., Geng, G., Feng, T., Zheng, B., Lu, Z.,
695   Streets, D. G., Ni, R., Brauer, M., van Donkelaar, A., Martin, R. V., Huo, H., Liu, Z.,
696   Pan, D., Kan, H., Yan, Y., Lin, J., He, K., and Guan, D.: Transboundary health impacts
697   of transported global air pollution and international trade, Nature, 543, 705–709,
698   https://doi.org/10.1038/nature21712, 2017.
699

700   Zheng, B., Tong, D., Li, M., Liu, F., Hong, C., Geng, G., Li, H., Li, X., Peng, L., Qi, J., Yan,
701   L., Zhang, Y., Zhao, H., Zheng, Y., He, K., and Zhang, Q.: Trends in China's
702   anthropogenic emissions since 2010 as the consequence of clean air actions, Atmos.
703   Chem. Phys., 18, 14095–14111, https://doi.org/10.5194/acp-18-14095- 2018, 2018.
704
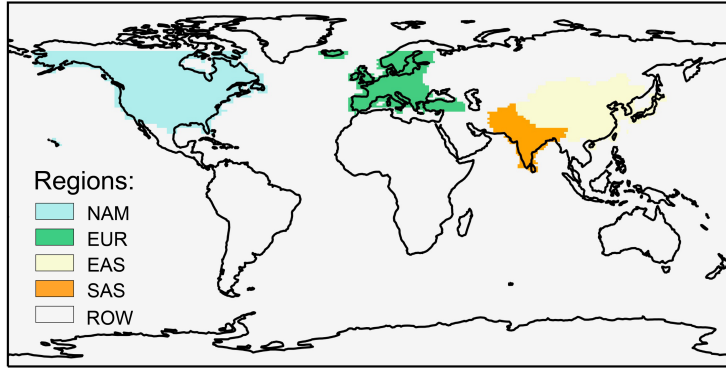
705

706 **Figure 1.** Tagged source regions (NAM: North America; EUR: Europe; EAS: East Asia; SAS:
707 South Asia; ROW: rest of the world).

708
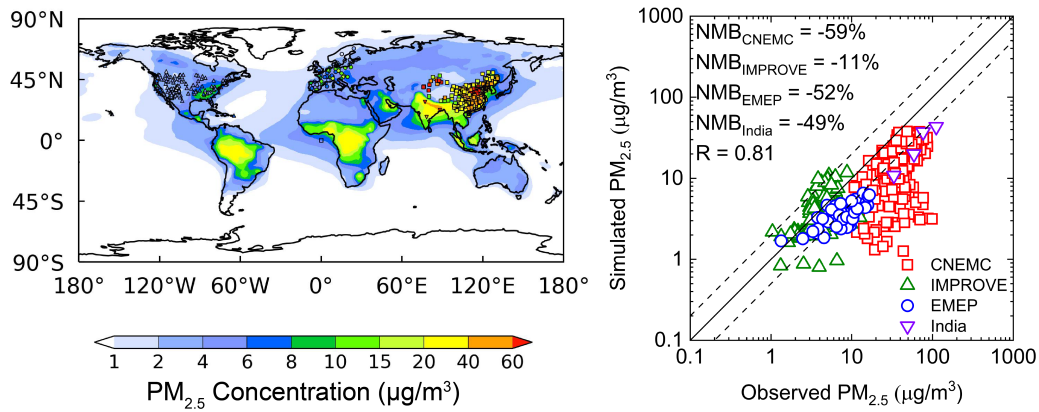
709 **Figure 2.** Spatial distribution (left panel) and scatter plot (right) between the simulated and
710 observed annual mean near-surface PM$_{2.5}$ concentrations (µg/m^3) in 2017. Observational data
711 are from IMPROVE (triangle), EMEP (circle), India (inverted triangle) and CNEMC (square).
712 The solid line marks the 1:1 ratio and dashed lines mark the 1:2 and 2:1 ratios. Normalized
713 mean bias (NMB) and correlation coefficient (R) between observation and simulation are
714 shown on the right panel. $NMB = 100\% \times \sum(M_i - O_i)/\sum O_i$, where M_i and O_i are the
715 modeled and observed values at site i , respectively.

716
717
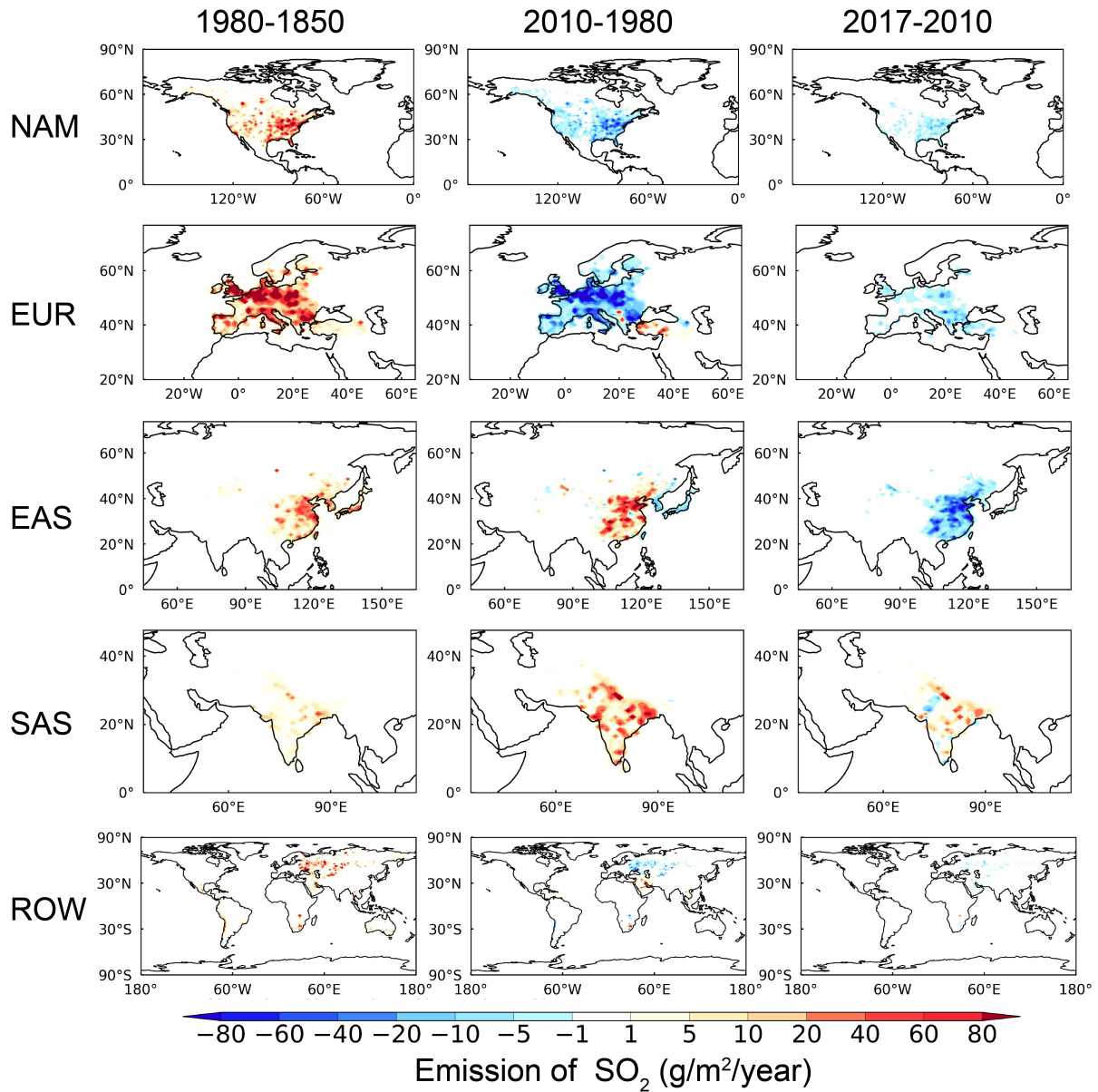
Figure 3. Changes in anthropogenic sulfur dioxide (SO_2) emissions ($g/m^2/year$) between 1850 and 1980 (left), between 1980 and 2010 (middle), and between 2010 and 2017 (right) in the 5 tagged source regions (NAM, EUR, EAS, SAS and ROW from top to bottom).

718

719

720

721

722

723

724
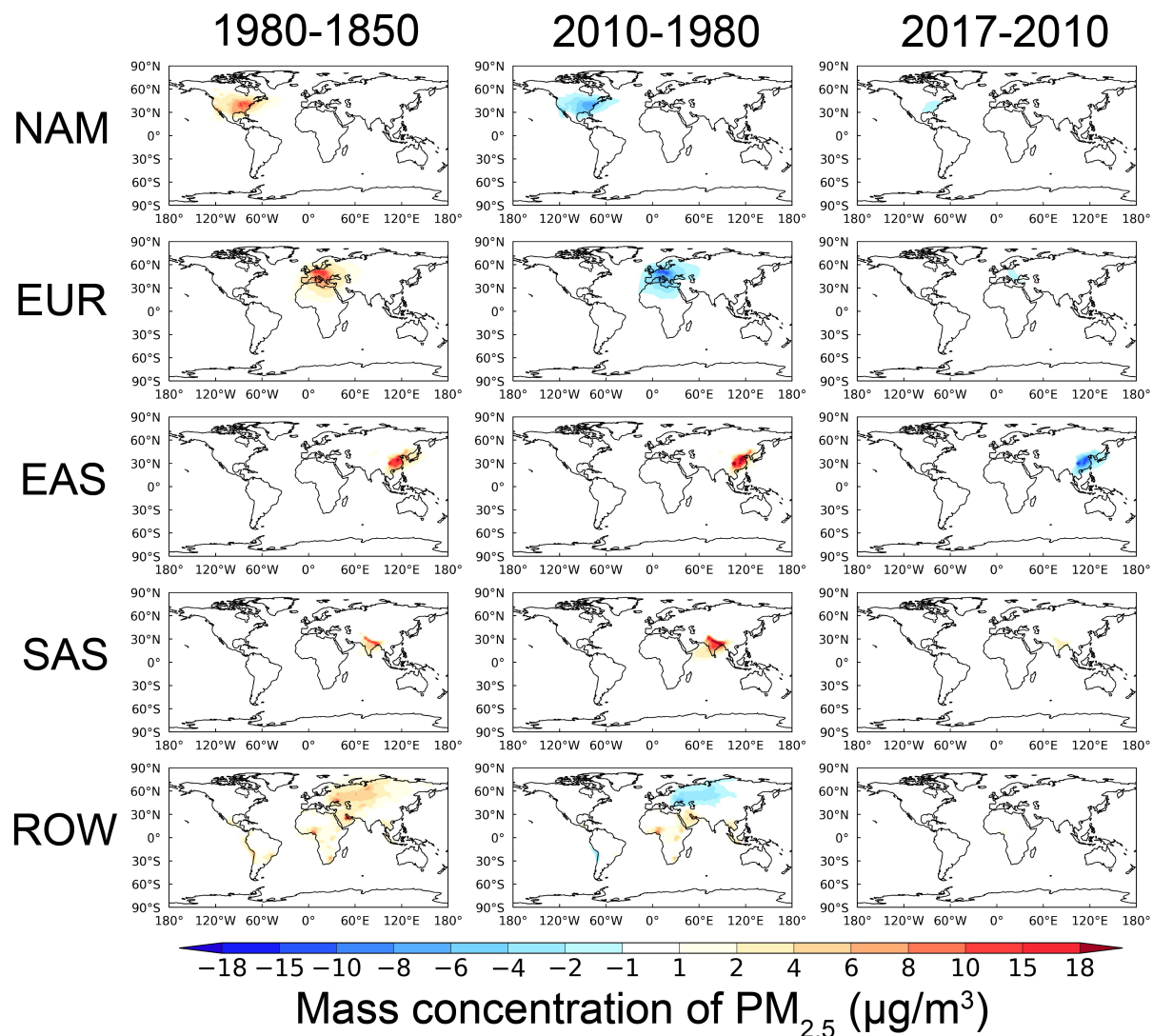
Figure 4. Changes in near-surface mass concentration (μg/m³) of anthropogenic PM₂.₅
contributed by the 5 tagged source regions (NAM, EUR, EAS, SAS and ROW from top to
bottom) between 1850 and 1980 (left), between 1980 and 2010 (middle), and between 2010
and 2017 (right).

729
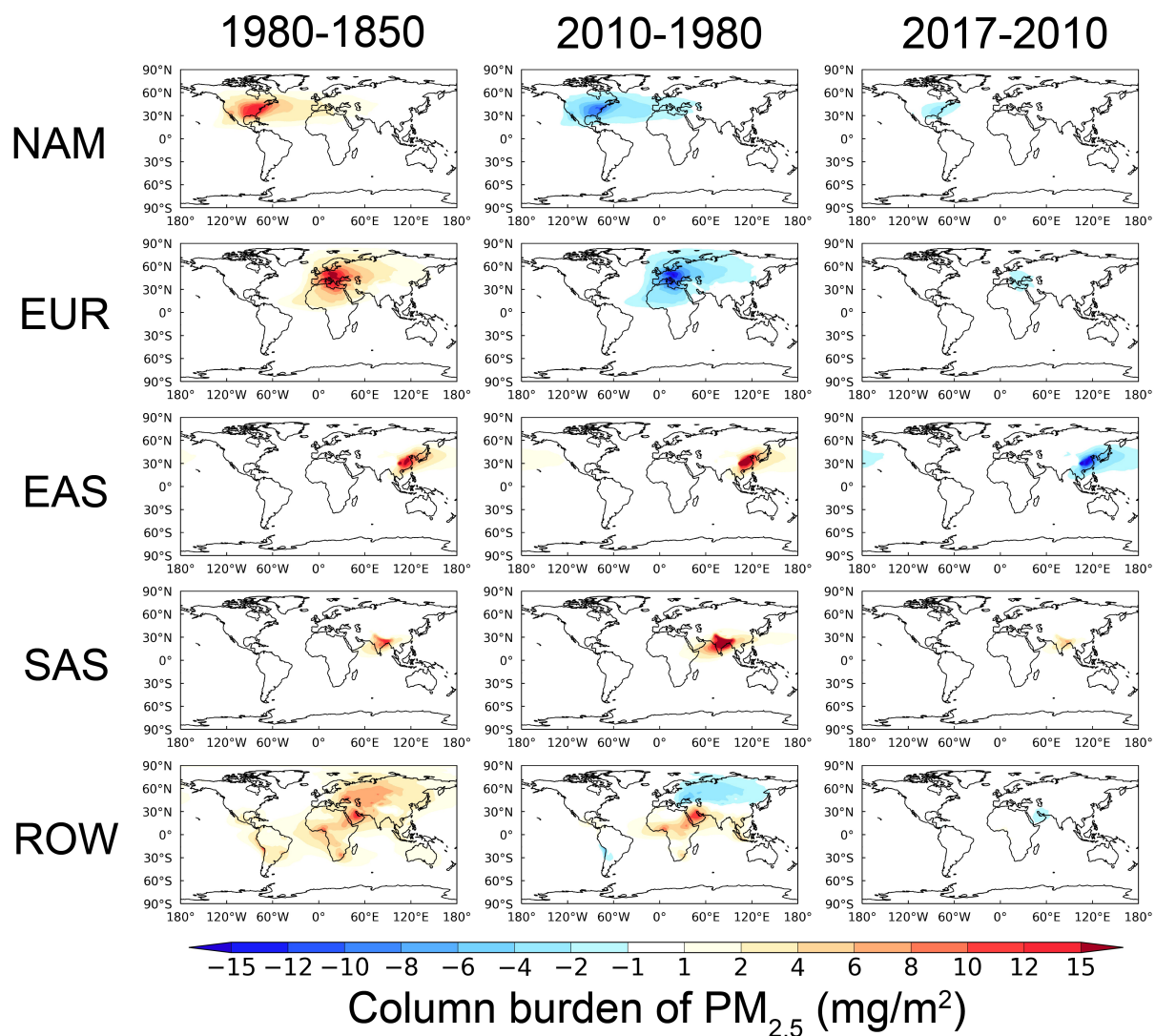
Figure 5. Changes in column burden (mg/m^2) of anthropogenic PM$_{2.5}$ contributed by the 5 tagged source regions (NAM, EUR, EAS, SAS and ROW from top to bottom) between 1850 and 1980 (left), between 1980 and 2010 (middle), and between 2010 and 2017 (right).
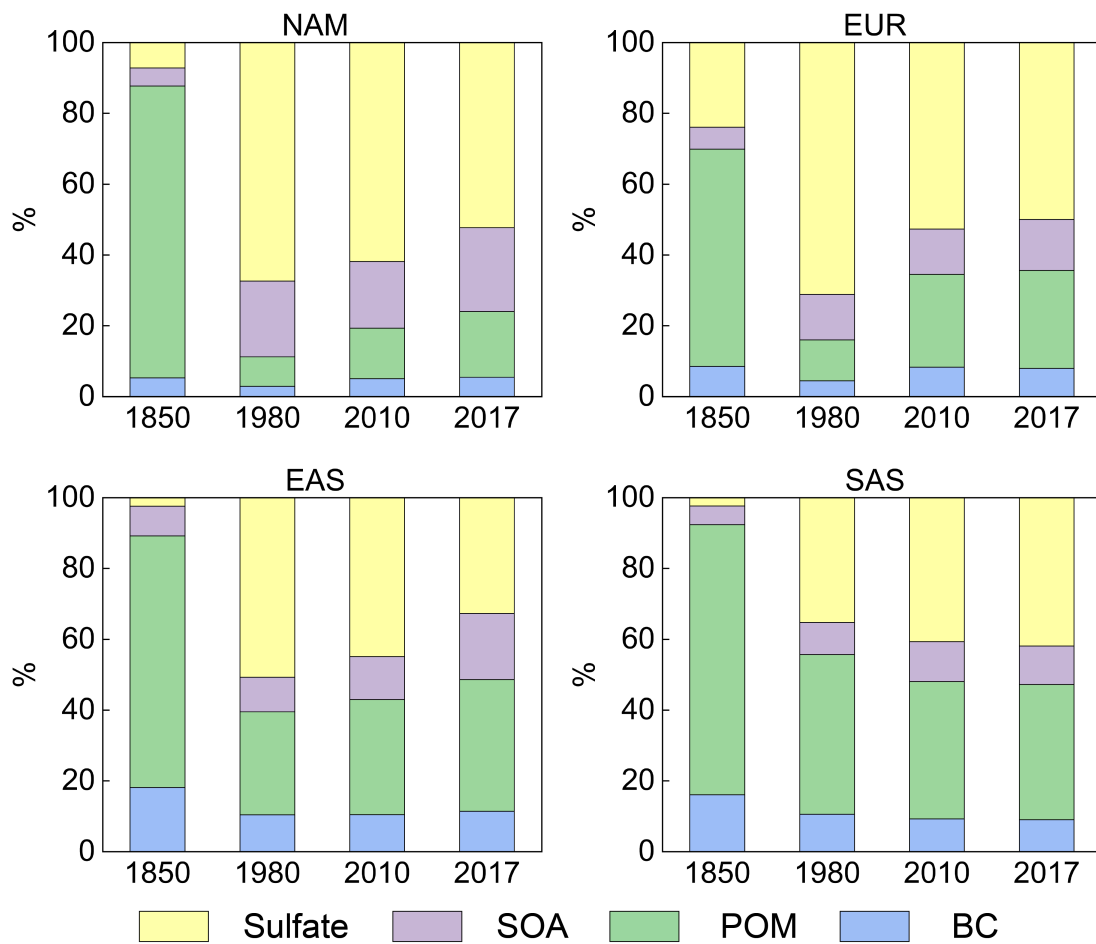
Figure 6. Percentage contributions (%) of aerosol species including BC, POM, SOA and sulfate to the near-surface mass concentrations of $PM_{2.5}$ averaged over the four major emission source regions (NAM, EUR, EAS and SAS) in the focused four years (1850, 1980, 2010 and 2017).
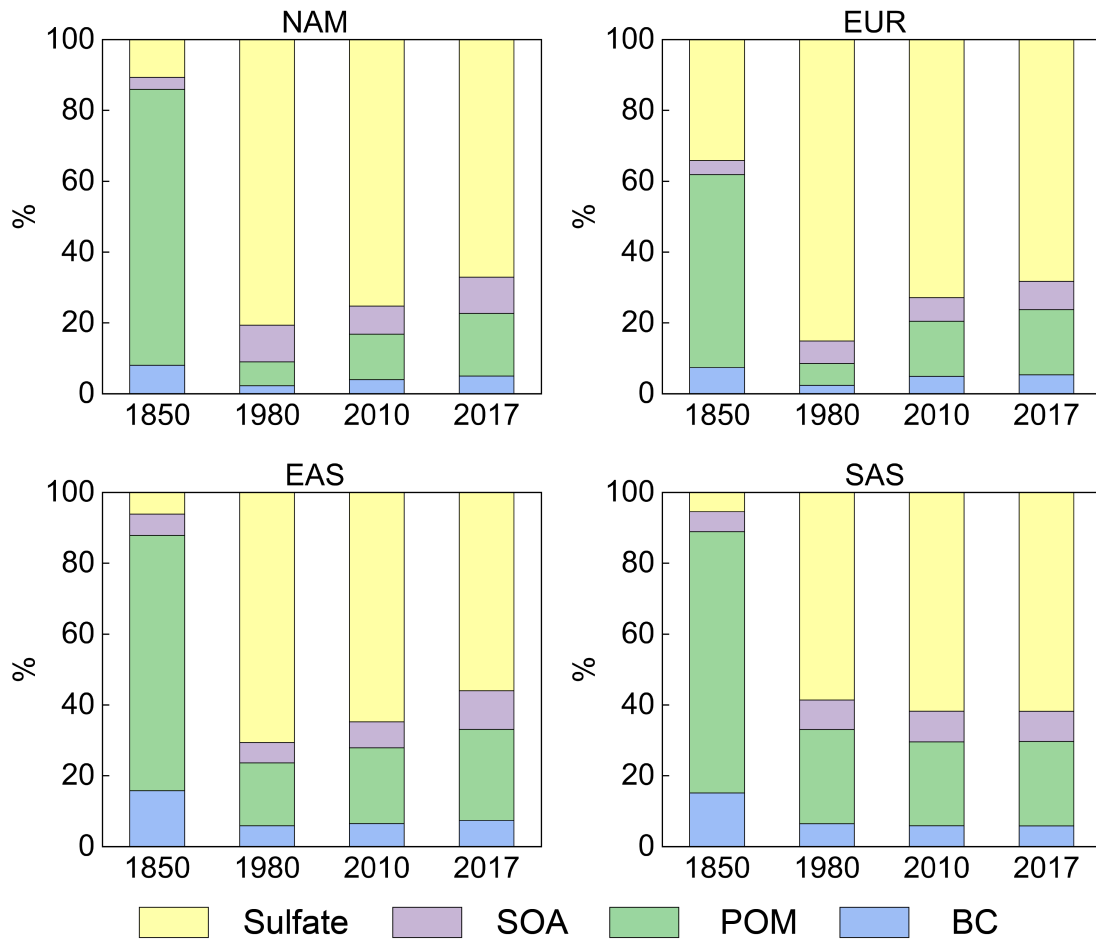
Figure 7. Percentage contributions (%) of aerosol species including BC, POM, SOA and sulfate to the column burden of $PM_{2.5}$ averaged over the four major emission source regions (NAM, EUR, EAS and SAS) in the focused four years (1850, 1980, 2010 and 2017).

746
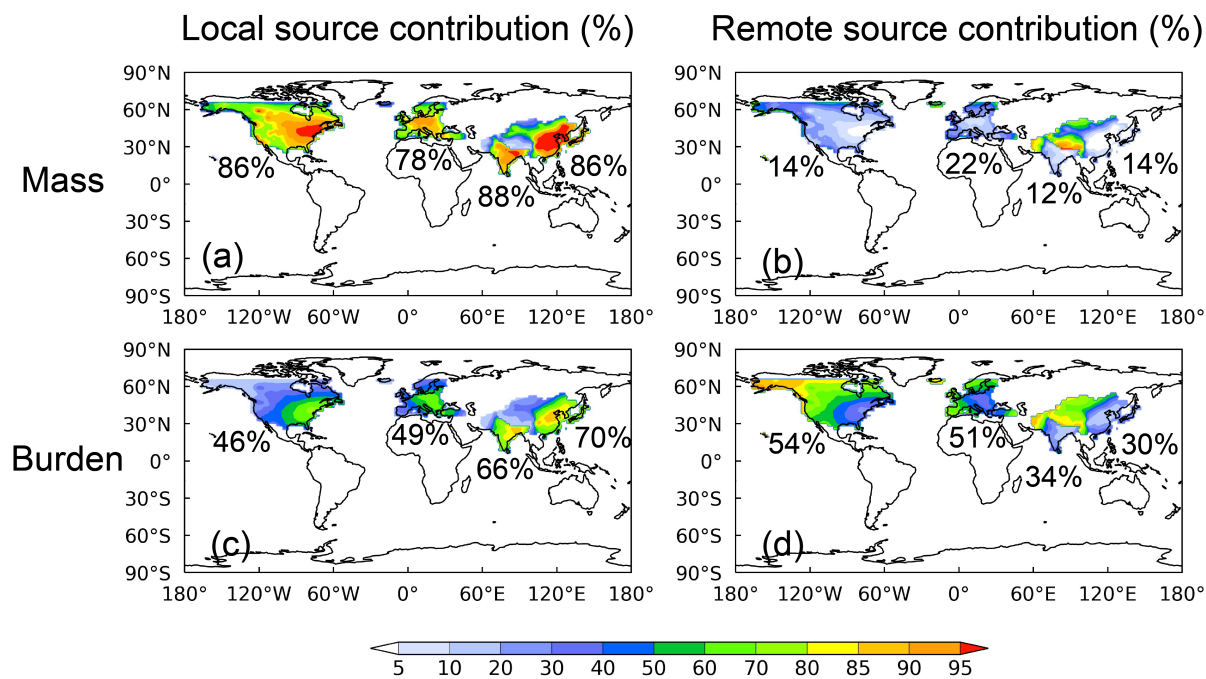
Figure 8. Relative contributions (%) from (a, c) local and (b, d) remote anthropogenic emissions to the near-surface mass concentrations and column burdens of PM$_{2.5}$ in the four targeted regions (NAM, EUR, EAS and SAS) in 2010. Numbers marked on the figure are the regional average over the four individual targeted regions.

751
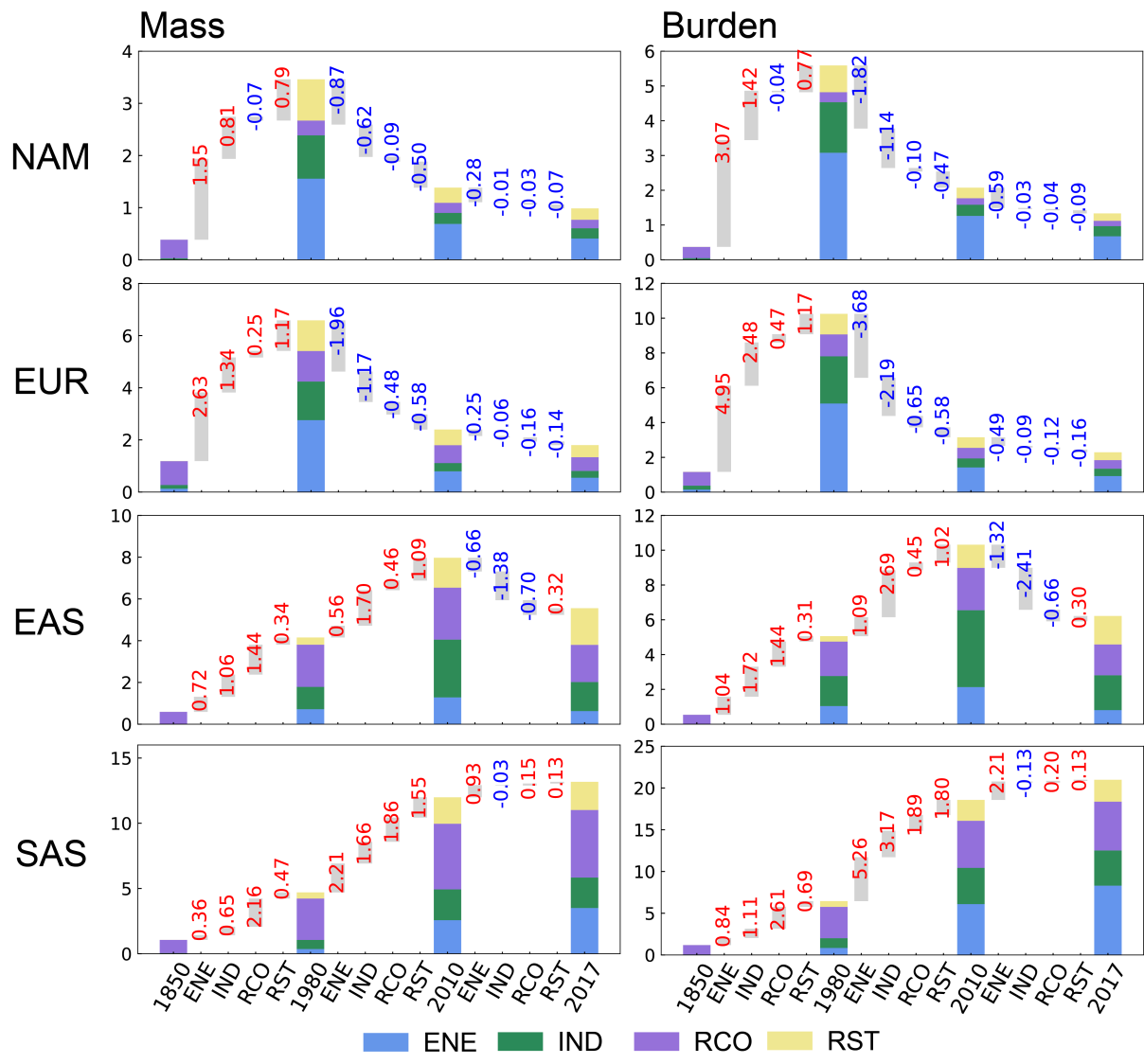
Figure 9. Local source contributions from four individual emission sectors (ENE, IND, RCO and RST) to the near-surface mass concentrations (μg/m^3, left) and column burdens (mg/m^2, right) of anthropogenic PM$_{2.5}$ in the four targeted regions (NAM, EUR, EAS and SAS from top to bottom) for years 1850, 1980, 2010 and 2017 (in color bars). Grey bar and numbers in between two years show the change in sector contributions. Positive values are shown in red and negative values are shown in blue.
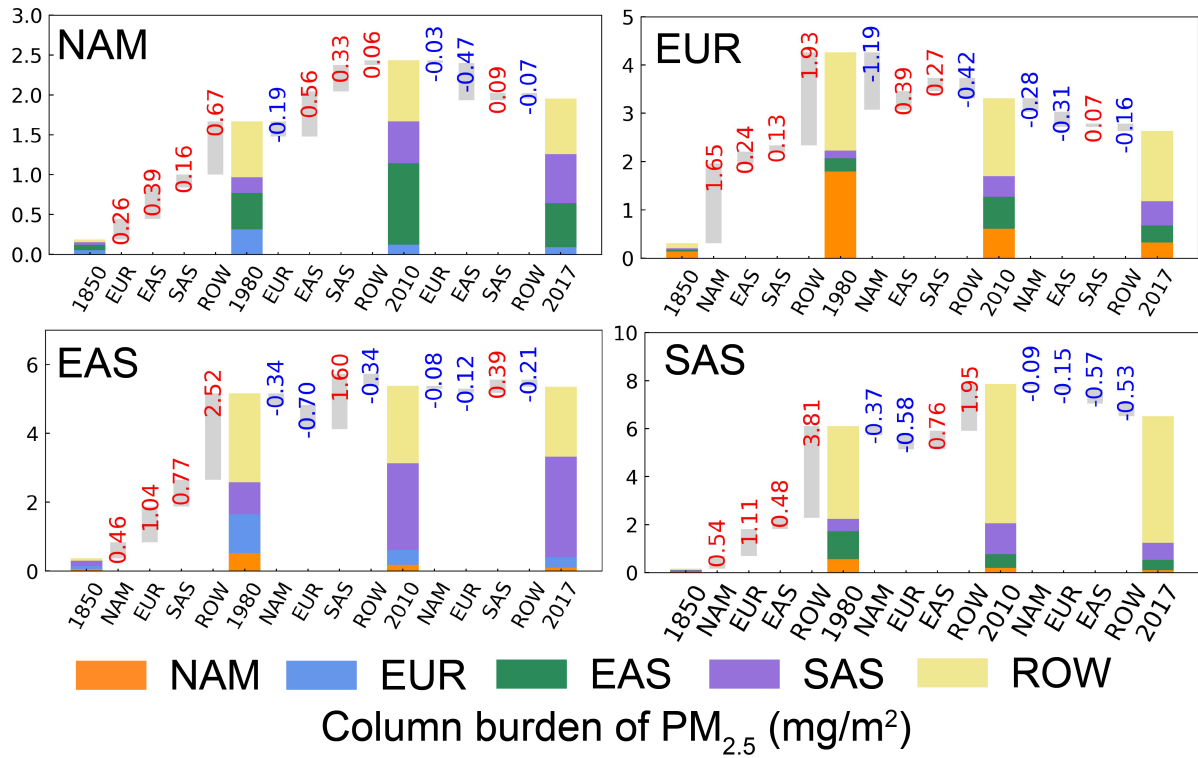
Figure 10. Same as Figure 9, but for contributions from the remote tagged source regions to the column burdens (mg/m²) of anthropogenic PM$_{2.5}$ in the four targeted regions (NAM, EUR, EAS and SAS).
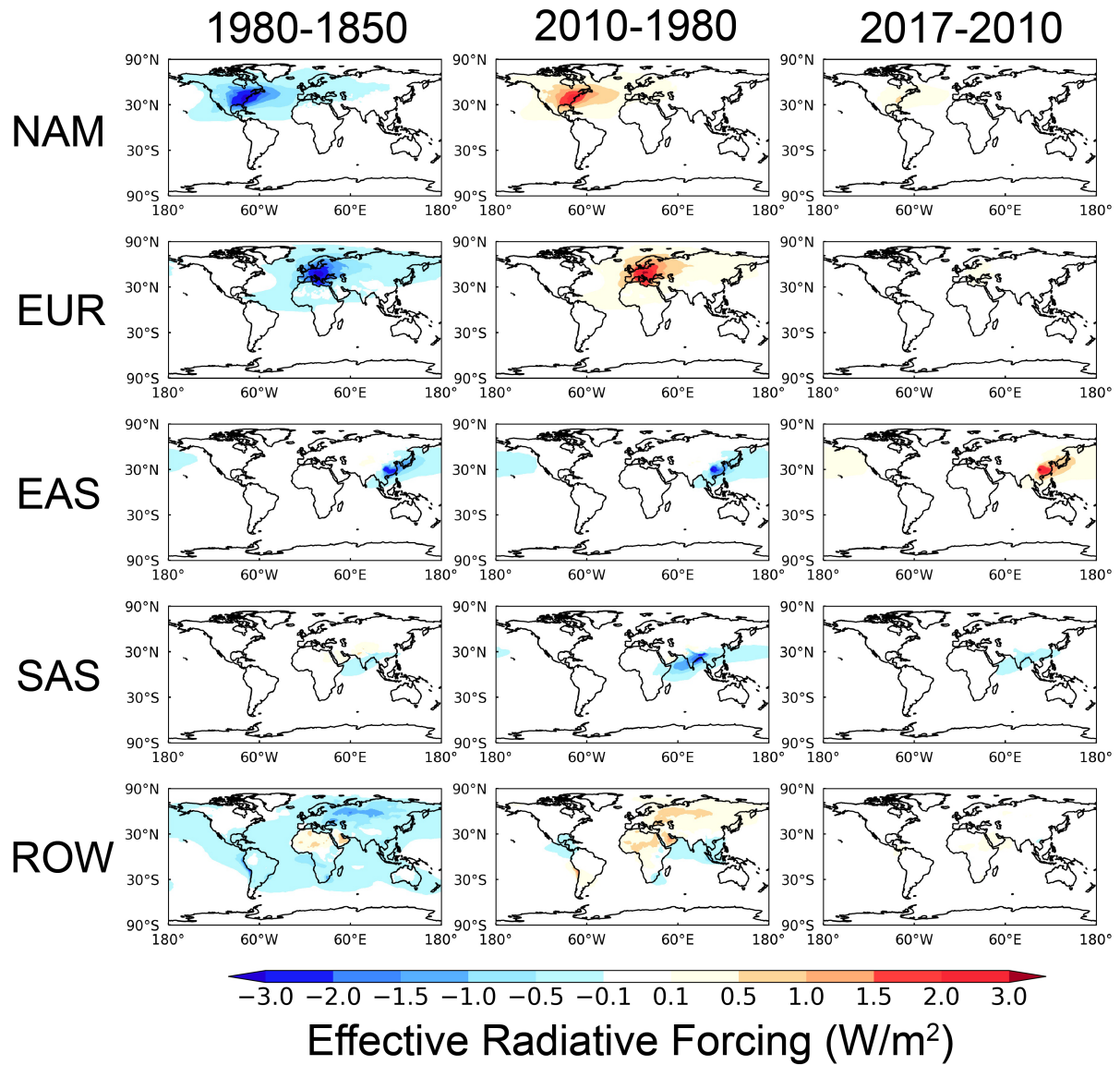
Figure 11. Changes in effective radiative forcing (W m^{-2}) at the top of the atmosphere due to aerosol-radiation interactions between 1850 and 1980 (left), between 1980 and 2010 (middle), and between 2010 and 2017 (right) attributed to the changes in anthropogenic emissions from NAM, EUR, EAS, SAS and ROW (from top to bottom).